Dipole response in neutron-rich nuclei with new Skyrme interactions

H. Zheng,[1,*] S. Burrello,[1,2] M. Colonna,[1] and V. Baran[3]
[1]*Laboratori Nazionali del Sud, INFN, I-95123 Catania, Italy*
[2]*Physics and Astronomy Department, University of Catania, Catania, Italy*
[3]*Faculty of Physics, University of Bucharest, Bucharest, Romania*
(Received 22 February 2016; revised manuscript received 18 May 2016; published 18 July 2016)

We investigate the isoscalar and isovector $E1$ response of neutron-rich nuclei, within a semiclassical transport model employing effective interactions for the nuclear mean field. In particular, we adopt the recently introduced SAMi-J Skyrme interactions, whose parameters are specifically tuned to improve the description of spin-isospin properties of nuclei. Our analysis evidences a relevant degree of isoscalar-isovector mixing of the collective excitations developing in neutron-rich systems. Focusing on the low-lying strength emerging in the isovector response, we show that this energy region essentially corresponds to the excitation of isoscalar-like modes, which also contribute to the isovector response owing to their mixed character. Considering effective interactions which mostly differ in the isovector channels, we observe that these mixing effects increase with the slope L of the symmetry energy at saturation density, leading to a larger strength in the low-energy region of the isovector response. This result appears connected to the increase, with L, of the neutron-proton asymmetry at the surface of the considered nuclei, i.e., to the neutron skin thickness.

DOI: 10.1103/PhysRevC.94.014313

I. INTRODUCTION

The dynamics of many-body interacting systems often manifests the development of collective patterns. The understanding of such fascinating properties of complex systems is quite helpful to shed light on fundamental properties of the interaction among the constituent particles. In particular, the investigation of collective phenomena represents one of the most challenging and lively research fields in nuclear physics. In nuclei, giant resonances are well established collective states, with an energy larger than the particle separation energy [1]. An example is the giant dipole resonance (GDR), which is still the object of intense investigation. With the advent of the first-generation exotic-beam facilities, much attention was directed towards the features of the collective (multipole) response of unstable nuclei. Restricting the discussion to isovector dipole excitations of neutron-rich systems, one generally observes a stronger fragmentation of strength than in nuclei with small neutron excess, with significant components located in an energy domain well below that of the GDR [2–11]. The nature of the low-lying excitations is still a matter of ongoing discussion [12–23]. Unlike the GDR, where neutrons and protons move against each other, this low-lying strength could be associated with an oscillation of the outermost neutrons (neutron skin) against the $N = Z$ core. This mode is commonly referred to as a "soft" or "pygmy" dipole resonance (PDR). This interpretation was already discussed in the early 1990s [24,25] and is supported by recent calculations based on the quasiparticle-phonon model [26,27], the relativistic quasiparticle random phase approximation (and extensions) [28–31], as well as by some nonrelativistic random phase approximation (RPA) studies [32,33]. On the other hand, other microscopic studies predict a larger fragmentation of the GDR strength [34] and the absence of collective states in the low-lying excitation region [13,35], thus relating the observed strength to a particular structure of the single-particle levels. Therefore a number of critical questions concerning the nature of the PDR still remain.

It is worth noting that the low-lying electric dipole $E1$ strength in unstable neutron-rich nuclei is currently discussed also in the astrophysical context, in connection with the reaction rates in the r-process nucleosynthesis. It appears that the existence of the pygmy mode could have a strong impact on the abundances of the elements in the Universe [36–39]. Moreover, as evidenced in mean-field based calculations, the features of neutron-rich nuclei, such as pygmy mode and neutron skin, are clearly related to the isovector terms of the nuclear effective interactions (or modern energy density functional theories). These terms are linked to the symmetry energy contribution in the nuclear equation of state (EoS), a concept which is widely employed in the description of heavy ion collisions [40–42] and also in astrophysics, as far as the modeling of supernova explosions and neutron stars is concerned [43–45].

The aim of the present paper is therefore to investigate the dipole response of neutron-rich nuclei, by solving the semiclassical Vlasov equation. In the past, studies based on semiclassical approaches, such as the Goldhaber-Teller (GT) [46] or the Steinwedel-Jensen (SJ) [47] models, have given an important contribution to the understanding of the main features of giant resonances and of their link to important nuclear properties, such as incompressibility and symmetry energy. In particular, the Vlasov equation has already been shown to describe reasonably well some relevant properties of different collective excitations of nuclei [48–50]. It is clear that, within such a semiclassical description, shell effects, certainly important in shaping the fine structure of the dipole response [34], are absent. However, the genuine collective features of the nuclear excitations should naturally come out from this analysis.

*zheng@lns.infn.it

Here, for the mean-field representation, we will employ new effective interactions of the Skyrme type—the SAMi-J interactions—which have been especially devised to improve the description of spin-isospin properties of nuclei [51]. We will focus on the mixed isoscalar-isovector character of the collective excitations in neutron-rich nuclei, in some analogy with features already discussed in the context of infinite nuclear matter, where the degree of mixing is observed to increase with the isospin asymmetry, tuned by the density dependence of the symmetry energy [40,41]. Then, we show that the relative isoscalar-isovector weight of the different modes, as observed in the nuclear response, is determined by their intrinsic structure, in terms of isoscalar (IS) and isovector (IV) components, as well as by the type of initial perturbation considered. As a result, within our framework, the low-lying strength arising in the IV dipole response essentially reflects the partial isovector character of collective modes which are mostly isoscalar-like, in agreement with previous semiclassical [52] and RPA [34] studies.

An important goal of our investigation is to get a deeper insight into the link between the nuclear response and the properties of the underlying effective interaction. In particular, considering SAMi-J parametrizations which mostly differ in the isovector channel, we will explore the relation between the mixed isoscalar-isovector structure of the dipole collective modes and the density dependence of the symmetry energy. We notice that the latter quantity also affects the size of the neutron skin. Thus our analysis also aims at elucidating the possible connection between the strength observed, for selected nuclei, in the PDR region and the corresponding neutron skin extension [53].

The paper is organized as follows: in Sec. II we outline the theoretical framework and the main ingredients associated with the Vlasov equation and its numerical solution. The different Skyrme parametrizations employed in our study are presented. The results concerning the isoscalar and isovector dipole response for selected nuclei in three different mass regions are discussed in Sec. III A. Two different kinds of initial perturbation, corresponding to standard isoscalar and isovector excitations, are considered. The corresponding transition densities are presented in Sec. III B. Finally, in Sec. IV, conclusions and perspectives are drawn.

II. THEORETICAL FRAMEWORK

The Vlasov equation, which describes the time evolution of the one-body distribution function in phase space, represents the semiclassical limit of the time-dependent Hartree-Fock (TDHF) method and, for small oscillations, of the RPA equations. While the model is unable to account for effects associated with the shell structure, this self-consistent approach is suitable to describe robust quantum modes, of zero-sound type, in both nuclear matter and finite nuclei [40,49,52,54]. One essentially has to solve the two coupled Vlasov kinetic equations for the neutron and proton distribution functions $f_q(\mathbf{r},\mathbf{p},t)$, with $q = n, p$ [40]:

$$\frac{\partial f_q}{\partial t} + \frac{\partial \epsilon_q}{\partial \mathbf{p}}\frac{\partial f_q}{\partial \mathbf{r}} - \frac{\partial \epsilon_q}{\partial \mathbf{r}}\frac{\partial f_q}{\partial \mathbf{p}} = 0. \tag{1}$$

In the equations above, ϵ_q represents the single-particle energy, which can be deduced from the energy density, $\mathscr{E}$. Considering a standard Skyrme interaction, the latter is expressed in terms of the isoscalar, $\rho = \rho_n + \rho_p$, and isovector, $\rho_3 = \rho_n - \rho_p$, densities and kinetic energy densities ($\tau = \tau_n + \tau_p$, $\tau_3 = \tau_n - \tau_p$) as [55]

$$\mathscr{E} = \frac{\hbar^2}{2m}\tau + C_0\rho^2 + D_0\rho_3^2 + C_3\rho^{\alpha+2} + D_3\rho^{\alpha}\rho_3^2 + C_{\text{eff}}\rho\tau + D_{\text{eff}}\rho_3\tau_3 + C_{\text{surf}}(\nabla\rho)^2 + D_{\text{surf}}(\nabla\rho_3)^2, \tag{2}$$

where m is the nucleon mass and the coefficients C and D with different indices are combinations of traditional Skyrme parameters. In particular, the terms with coefficients C_{eff} and D_{eff} are the momentum-dependent contributions to the nuclear effective interaction. The Coulomb interaction is also considered in the calculations. We are mostly interested in the effects linked to the isovector terms, thus we introduce the symmetry energy per nucleon, $E_{\text{sym}}/A = C(\rho)I^2$, where $I = (N - Z)/A$ is the asymmetry parameter and the coefficient $C(\rho)$ can be written as a function of the Skyrme coefficients (at temperature $T = 0$):

$$C(\rho) = \frac{\epsilon_F}{3} + D_0\rho + D_3\rho^{\alpha+1} + \frac{2m}{\hbar^2}\left(\frac{C_{\text{eff}}}{3} + D_{\text{eff}}\right)\epsilon_F\rho, \tag{3}$$

with ϵ_F denoting the Fermi energy at density ρ.

In the following we will adopt the recently introduced SAMi-J Skyrme effective interactions [51]. The corresponding parameters have been fitted based on the SAMi fitting protocol [51]: binding energies and charge radii of some doubly magic nuclei which allow the SAMi-J family to predict a reasonable saturation density ($\rho_0 = 0.159$ fm^{-3}), energy [$E/A(\rho = \rho_0) = -15.9$ MeV], and incompressibility ($K = 245$ MeV) of symmetric nuclear matter; some selected spin-orbit splittings; the spin and spin-isospin sensitive Landau Migdal parameters [56]; and, finally, the neutron matter EoS of Ref. [57]. These features allow the new SAMi interactions to give a reasonable description of isospin as well as spin-isospin resonances, keeping a good reproduction of well known empirical data such as masses, radii, and important nuclear excitations. The main difference between SAMi and the SAMi-J family is that SAMi-J has been produced by systematically varying the value of $J = C(\rho_0)$ from 27 to 35 MeV, keeping fixed the optimal value of the incompressibility and effective mass predicted by SAMi and refitting again the parameters for each value of J. This produces a set of interactions of similar quality on the isoscalar channel and that, approximately, isolates the effects of modifying the isovector channel in the study of a given observable. In our calculations, we employed, in particular, three SAMi-J parametrizations: SAMi-J27, SAMi-J31, and SAMi-J35 [51]. Since, as mentioned above, the SAMi-J interactions have been fitted in order to also reproduce the main features of finite nuclei, for the three parametrizations the symmetry energy coefficient gets the same value, $C(\rho_c) \approx 22$ MeV at $\rho_c = 0.65\rho_0$, which can be taken as the average density of medium-size nuclei. Thus the curves representing the density dependence of $C(\rho)$ cross each other at $\rho = \rho_c$,

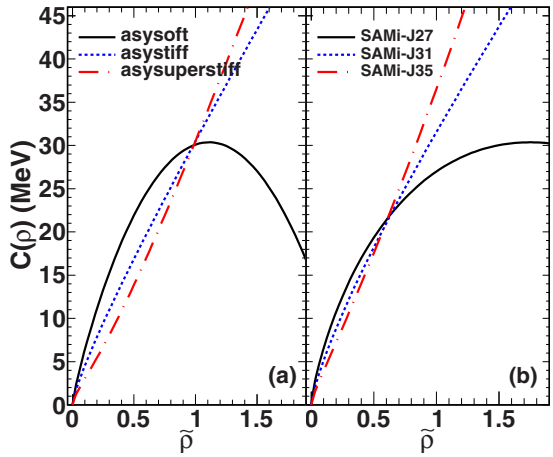

FIG. 1. The symmetry energy versus reduced density $\tilde{\rho} = \frac{\rho}{\rho_0}$ for the EoS without (a) and with (b) momentum-dependent terms.

i.e., below saturation density; see Fig. 1(b). The corresponding values of symmetry energy at saturation, together with the values of the slope parameter $L = 3\rho_0 \frac{dC(\rho)}{d\rho}|_{\rho=\rho_0}$ are reported in Table I. In the following we will also indicate the SAMi-J interactions as momentum-dependent (MD) interactions.

In order to make a connection with previous studies, we shall also consider simplified Skyrme interactions where the momentum dependent terms are neglected ($C_{\rm eff} = D_{\rm eff} = 0$), corresponding to an incompressibility modulus equal to $K = 200$ MeV [53]. We will refer to these interactions as momentum-independent (MI) interactions.

As far as the symmetry energy is concerned, the parametrizations considered allow for three different types of density dependence, associated with three different parametrizations of the potential part of the symmetry energy coefficient, $C_{\rm pot}(\rho)$. For the *asystiff* EoS, $C_{\rm pot}(\rho) = 18\rho/\rho_0$ MeV. The *asysoft* case corresponds to a SKM* Skyrme-like parametrization with $C_{\rm pot}(\rho) = 0.5\rho(482 - 1638\rho)$ MeV, associated with a small value of the slope parameter L. Lastly, for the *asysuperstiff* EoS, $C_{\rm pot}(\rho) = 18\frac{\rho}{\rho_0}\frac{2\rho}{(\rho+\rho_0)}$ MeV, the symmetry term increases rapidly around saturation density, being characterized by a large value of the slope parameter. The corresponding values are listed in Table I. As one can see from Fig. 1(a), the three parametrizations of the symmetry energy cross each other at $\rho = \rho_0$ in this case.

The integration of the transport equations is based on the test-particle (t.p.) (or pseudoparticle) method [58], with a number of 1500 t.p. per nucleon in all the cases, ensuring in this way a good spanning of the phase space. In order to determine the ground state configuration of the nuclei under study, one should find the stationary solution of Eq. (1). We adopt the following numerical procedure: neutrons and protons are distributed inside spheres of radii R_n and R_p, respectively. Accordingly, particle momenta are initialized inside Fermi spheres associated with the local neutron or proton densities. Then R_n and R_p are tuned in order to minimize the corresponding total energy, associated with the effective interaction adopted in the calculations. We note here that the test-particle method is able to reproduce accurately the equation of state of nuclear matter and provide reliable results regarding the properties of nuclear surface [59] and ground state energy for finite nuclei [53,60].

From the one-body distribution functions one obtains the local densities:

$$\rho_q(\mathbf{r},t) = \frac{2}{(2\pi\hbar)^3}\int d^3p\, f_q(\mathbf{r},\mathbf{p},t), \tag{4}$$

as well as the average value of the radial distance $\mathbf{r}$ to the power n:

$$\langle \mathbf{r}_q^n \rangle = \frac{1}{N_q}\int d^3r\, \mathbf{r}^n \rho_q(\mathbf{r},t). \tag{5}$$

In the above equation, $N_n = N$ and $N_p = Z$ denote neutron and proton number, respectively. As we will see, these quantities are quite useful in the following analysis (see Sec. III).

Because test particles are often associated with finite width wave packets (we use triangular functions [61]), some surface effects are automatically included in the initialization procedure and in the dynamics, even though explicit surface terms, such as those contained in the effective Skyrme interactions, are not considered. This implies that, for the surface terms, one cannot simply use the coefficients associated with the SAMi-J parametrizations. Indeed we observe that a good reproduction of the experimental values of the proton root-mean-square radius and binding energy, for the nuclei selected in our analysis, is obtained when taking $C_{\rm surf} = D_{\rm surf} = 0$ in our parametrizations. Thus this choice has been adopted in the following.

We will concentrate our analysis on three mass regions, considering the following neutron-rich nuclei: ^{68}Ni ($N/Z = 1.43$), ^{132}Sn ($N/Z = 1.64$), ^{208}Pb ($N/Z = 1.54$). The corresponding values of binding energy and the neutron and proton root-mean-square radii are reported in Tables II, III, and IV, for the SAMi-J interactions. In Fig. 2, we show the neutron and proton density profiles, obtained for the system ^{132}Sn, with the three SAMi-J parametrizations considered in our study. According to the procedure adopted here to build the ground state configuration, these values are not supposed to coincide with the results of Hartree-Fock calculations, but

TABLE I. The symmetry energy coefficient at saturation density for the Skyrme interactions employed in our study and the corresponding slope L.

Interaction	$C(\rho_0)$ (MeV)	L (MeV)	Interaction	$C(\rho_0)$ (MeV)	L (MeV)
asysoft	30	14.8	SAMi-J27	27	29.9
asystiff	30.5	79	SAMi-J31	31	74.5
asysuperstiff	30.5	106	SAMi-J35	35	115.2

TABLE II. Neutron and proton root-mean-square radii, and their difference, and binding energy for ^{68}Ni, as obtained with the SAMi-J interactions. The experimental values, for charge radius and binding energy, are also indicated (from [62]).

Interaction	$\sqrt{\langle r^2\rangle_n}$ (fm)	$\sqrt{\langle r^2\rangle_p}$ (fm)	$\sqrt{\langle r^2\rangle_n} - \sqrt{\langle r^2\rangle_p}$ (fm)	BE/A (MeV)
SAMi-J27	4.043	3.889	0.154	−9.130
SAMi-J31	4.102	3.898	0.204	−9.050
SAMi-J35	4.143	3.900	0.243	−8.971
^{68}Ni expt.		3.857 (^{64}Ni)		−8.682

they are actually quite close [63]. As expected, the neutron skin thickness increases with the slope parameter L: this effect is indeed related to the derivative of the symmetry energy around saturation density. When the symmetry energy decreases significantly below ρ_0, as in the case of the *asysuperstiff* EoS or the SAMi-J35 interaction, it is energetically convenient for the system to push the neutron excess towards the nuclear surface.

The same trend is observed for the ^{68}Ni and ^{208}Pb ground state configuration (see Tables II and IV) and also for the MI interactions [53]. However, it should be noticed that, in the case of the SAMi-J interactions, the different value of the symmetry energy at saturation induces a quite different behavior of the neutron density also in the bulk; see Fig. 2.

III. RESULTS

A. Collective dipole response

We study the $E1$ (isoscalar and isovector) response of nuclear systems, considering initial conditions determined by the instantaneous excitation $V_{\rm ext} = \eta_k \delta(t - t_0)\hat{D}_k$, at $t = t_0$, along the z direction [54,64]. Here $\hat{D}_k$ denotes the operator employed to introduce isoscalar ($k = $ S) or isovector ($k = $ V) dipole excitations:

$$\hat{D}_S = \sum_i \left(r_i^2 - 5/3\langle r^2\rangle\right) z_i, \tag{6}$$

$$\hat{D}_V = \sum_i \tau_i N/A z_i - (1-\tau_i) Z/A z_i, \tag{7}$$

where $\tau_i = 1$ (0) for protons (neutrons) and $\langle r^2\rangle$ denotes the mean square radius of the nucleus considered. We note that the operator $\hat{D}_V$ also contains an isoscalar component, which vanishes only for symmetric ($N = Z$) systems. According to basic quantum mechanics, if $|\Phi_0\rangle$ is the state before perturbation, then the excited state becomes $|\Phi_k(t_0)\rangle = e^{i\eta_k \hat{D}_k}|\Phi_0\rangle$. The value of η_k can be related to the initial expectation value of the collective dipole momentum $\hat{\Pi}_k$, which is canonically conjugated to the collective coordinate $\hat{D}_k$, i.e., $[\hat{D}_k, \hat{\Pi}_k] = i\hbar$ [65].

For instance, in the simpler case of the isovector excitation, $\hat{\Pi}_V$ is canonically conjugated to the collective coordinate $\hat{D}_V = (NZ/A)\hat{X}_V$, where $\hat{X}_V$ defines the distance between the center of mass (CM) of protons and the CM of neutrons. Then one obtains

$$\langle \Phi_V(t_0)|\hat{\Pi}_V|\Phi_V(t_0)\rangle = \eta_V \frac{NZ}{A}. \tag{8}$$

More generally, the dipole momentum is connected to the velocity field, which can be extracted by taking the spatial derivatives of the perturbation $V_{\rm ext}$ [52].

The strength function $S_k(E) = \sum_{n>0} |\langle n|\hat{D}_k|0\rangle|^2 \delta(E - (E_n - E_0))$, where E_n is the excitation energy of the state $|n\rangle$ and E_0 is the energy of the ground state $|0\rangle = |\Phi_0\rangle$, is obtained from the imaginary part of the Fourier transform of the time-dependent expectation value of the dipole moment $D_k(t) = \langle \Phi_k(t)|\hat{D}_k|\Phi_k(t)\rangle$ as

$$S_k(E) = \frac{{\rm Im}[D_k(\omega)]}{\pi \eta_k}, \tag{9}$$

where $D_k(\omega) = \int_{t_0}^{t_{\rm max}} D_k(t) e^{i\omega t} dt$, with $E = \hbar\omega$.

Dipole oscillations and response functions can be investigated, within our semiclassical treatment, considering a gentle perturbation of the ground state configuration of the nucleus under consideration and then looking at its dynamical evolution, as given by Eq. (1). We follow the dynamics of the system until $t_{\rm max} = 1800$ fm/c, thus being able to extract time oscillations of the dipole moments. A filtering procedure, as described in [66], was applied in order to eliminate the artifacts resulting from a finite time domain analysis of the signal. Thus a smooth cutoff function was introduced such that $D_k(t) \to D_k(t)\cos^2(\frac{\pi t}{2t_{\rm max}})$.

As is well known, in symmetric nuclear matter isoscalar and isovector modes are fully decoupled. However, in neutron-rich systems, neutrons and protons may oscillate with different amplitudes, thus inducing a coupling of isoscalar and isovector excitations. One of the main goals of our analysis is to get

TABLE III. The data for ^{132}Sn, similar to Table II.

Interaction	$\sqrt{\langle r^2\rangle_n}$ (fm)	$\sqrt{\langle r^2\rangle_p}$ (fm)	$\sqrt{\langle r^2\rangle_n} - \sqrt{\langle r^2\rangle_p}$ (fm)	BE/A (MeV)
SAMi-J27	4.940	4.728	0.212	−8.637
SAMi-J31	5.035	4.741	0.294	−8.552
SAMi-J35	5.150	4.753	0.397	−8.405
^{132}Sn expt.		4.7093		−8.354

TABLE IV. The data for ^{208}Pb, similar to Table II.

Interaction	$\sqrt{\langle r^2\rangle_n}$ (fm)	$\sqrt{\langle r^2\rangle_p}$ (fm)	$\sqrt{\langle r^2\rangle_n} - \sqrt{\langle r^2\rangle_p}$ (fm)	BE/A (MeV)
SAMi-J27	5.648	5.513	0.135	−8.105
SAMi-J31	5.735	5.536	0.198	−8.042
SAMi-J35	5.813	5.549	0.264	−7.930
^{208}Pb expt.		5.5012		−7.867

a deeper insight into this effect. Indeed it appears that, by considering an initial isovector perturbation of the system, one also gets an isoscalar response, and vice versa. This is illustrated in Fig. 3, where we represent dipole oscillations (left panels) and corresponding strength, as a function of the excitation energy E (right panels) for the system ^{132}Sn and the SAMi-J31 interaction, obtained by considering an initial IS perturbation with $\eta_S = 0.5$ MeV fm^{-2} [panels from (a) to (d)] or an initial IV perturbation with $\eta_V = 25$ MeV [panels from (e) to (h)].

One can observe that, when introducing an IS perturbation at the initial time t_0 [Fig. 3, panels (a) and (b)], also isovector-like modes are excited, as evidenced from the analysis of the corresponding isovector dipole oscillations and associated strength [panels (c) and(d)]. Similarly, an initial IV perturbation [panels (e) and (f)] also generates an isoscalar response [panels (g) and (h)].

In the isovector response [panel (f)] one can easily recognize the main IV GDR peak, with $E_{\rm GDR} \approx 14$ MeV. Some strength is also evidenced at lower energy (mostly in the range between $E_1 = 9$ MeV and $E_2 = 11$ MeV), which could be associated with the PDR. These low-energy modes contribute significantly to the corresponding isoscalar projection [panel (h)], now acquiring a larger strength, comparable to that associated with the robust GDR mode, thus manifesting their isoscalar-like nature. A (negative) peak is seen at higher energy (around 29 MeV), which corresponds to the giant isoscalar-like dipole mode (IS GDR) [34] which is also excited, owing to its mixed character, by the initial perturbation.

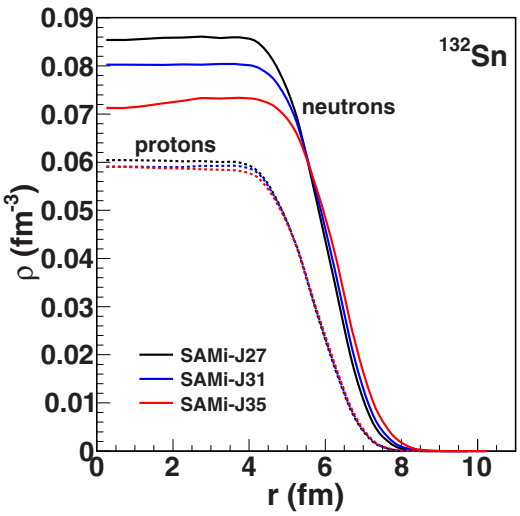

FIG. 2. The neutron (full lines) and proton (dashed lines) density profiles of ^{132}Sn for the SAMi-J27, SAMi-J31, and SAMi-J35 parametrizations.

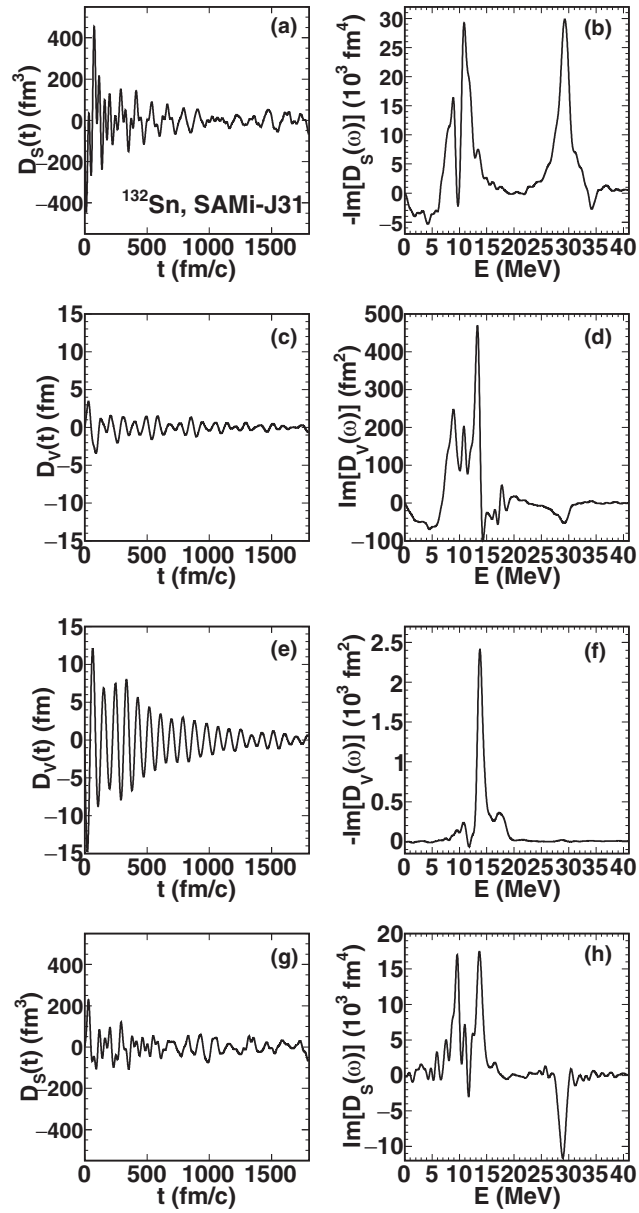

FIG. 3. The dipole oscillations (left panels) and corresponding strength (right panels) for ^{132}Sn and the SAMi-J31 interaction. Panels from (a) to (d) represent the results obtained with the initial IS perturbation and panels from (e) to (h) show the results obtained with the initial IV perturbation.

When agitating the system with an initial isoscalar excitation, essentially the same oscillation modes emerge, with a larger strength for the isoscalar-like ones in this case. Indeed, in the isoscalar response [panel (b)] two main peaks, whose positions are quite close to the E_1 and E_2 energies evidenced in panel (h), are observed in the low-energy region, together with some (smaller) strength located around the IV GDR region ($E_{\mathrm{GDR}} \approx 14$ MeV). A quite large contribution appears also in the high-energy region of the spectrum ($E \approx 29$ MeV). Projecting onto the isovector direction [panel (d)] the strength of the IV GDR mode is enhanced, as expected according to its isovector-like nature, becoming comparable to that of the low-energy isoscalar-like modes excited by the initial perturbation. On the other hand, the high-energy mode exhibits a quite small (negative) strength, pointing again to its isoscalar-like character.

To summarize, we observe that the same energy modes, which are actually the normal modes of the system and are of mixed nature, appear at the same time in the isoscalar and isovector responses of the system, but with a different weight, depending on their intrinsic structure and on the initial perturbation type. In particular, the low-energy modes, lying below the GDR peak, have predominant isoscalar nature, but they may also contribute to the isovector response in the PDR region.

We move now to investigate how the response of the system depends on the effective interaction adopted, in the three mass regions considered in this work. Hereafter we will only examine the isoscalar (isovector) response connected to an initial isoscalar (isovector) perturbation.

In Fig. 4(a) we show, for ^{68}Ni, the strength function corresponding to the IS dipole response as a function of the excitation energy E. In Fig. 4(b), the same quantity is shown but for the IV dipole response. In the case of ^{132}Sn and ^{208}Pb, the strength functions for the dipole response are depicted in Figs. 5(a) and 6(a) (IS) and in Figs. 5(b) and 6(b) (IV), respectively. In all panels, the predictions of the three selected SAMi-J interactions are shown.

For ^{68}Ni and ^{132}Sn, the isoscalar strength [panels (a)] appears quite fragmented in the low-energy domain. However, one can recognize two main regions of important contribution for all the interactions considered (see in particular the SAMi-J35 results) and identify a smaller peak centered at the energy of the IV GDR (originating from its mixed nature in neutron-rich systems, as stressed above). It is worth noting that the observation of two main low-energy peaks in the isoscalar response is in agreement with the semiclassical studies of Ref. [52], where isoscalar toroidal excitations are investigated. In particular, in [52] it is shown that the lowest energy mode is associated mostly with surface oscillations and, in the case of neutron-rich systems, is responsible for the low-lying strength observed in the isovector response (in the PDR region). On the other hand, RPA calculations [23,34] exhibit a more isolated peak in the low-energy region of the IS strength function $S_S(E)$, but some contributions appear also at higher energy, with respect to our calculations, in a region around the domain of the IV GDR (for instance, around 14 MeV in the ^{132}Sn case or around 13 MeV in the ^{208}Pb case [23]). This latter component of the IS dipole response has been

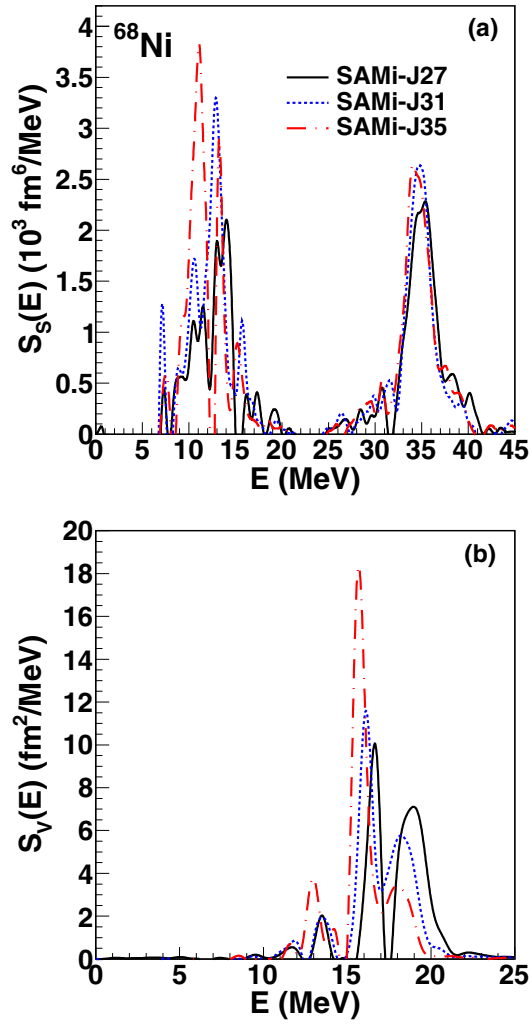

FIG. 4. The strength functions versus excitation energy for ^{68}Ni with SAMi-J27, SAMi-J31, and SAMi-J35 interactions. Panel (a) is for the initial IS perturbation and panel (b) is for the initial IV perturbation.

the object of several experimental and theoretical analyses [67]. These studies have pointed out the non-compressional nature of this excitation, in agreement with the findings, based on semiclassical studies, of Ref. [52].

For the largest system considered, ^{208}Pb, our calculations show just one main peak, of significant strength, in the low-energy region.

The discrepancy with respect to RPA calculations may be probably attributed to the lack of intrinsic gradient terms of quantal nature in our approach and to the numerical treatment of surface effects [68]. It appears more critical in smaller systems, where the relative importance of surface to volume effects increases.

In any case, the low-energy peaks of the IS response appear connected to the low-lying strength observed in the IV response [panels (b)], in the PDR region. Since the different peaks are quite close to each other, only one main peak, resulting from two interfering contributions, may appear in the PDR region of the IV response.

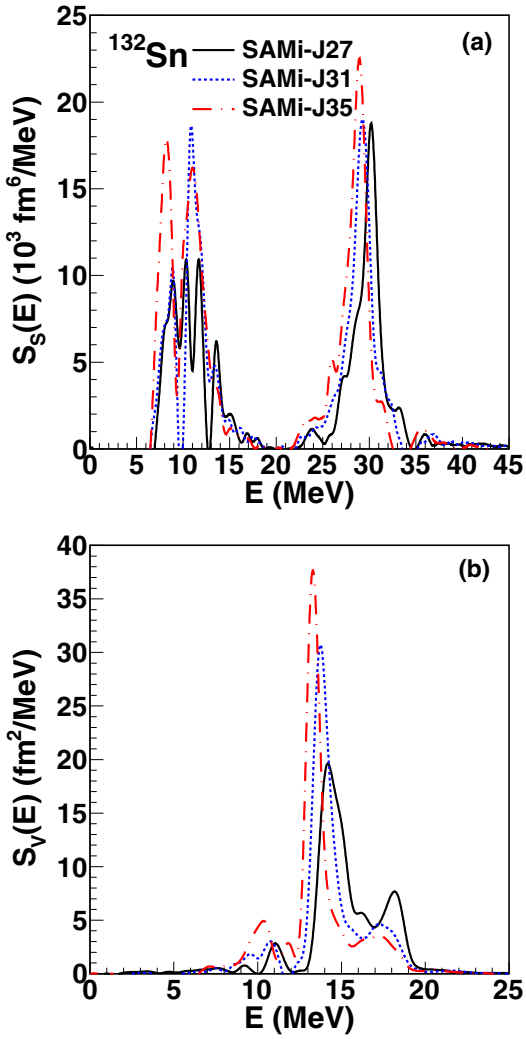

FIG. 5. Similar to Fig. 4 but for ^{132}Sn.

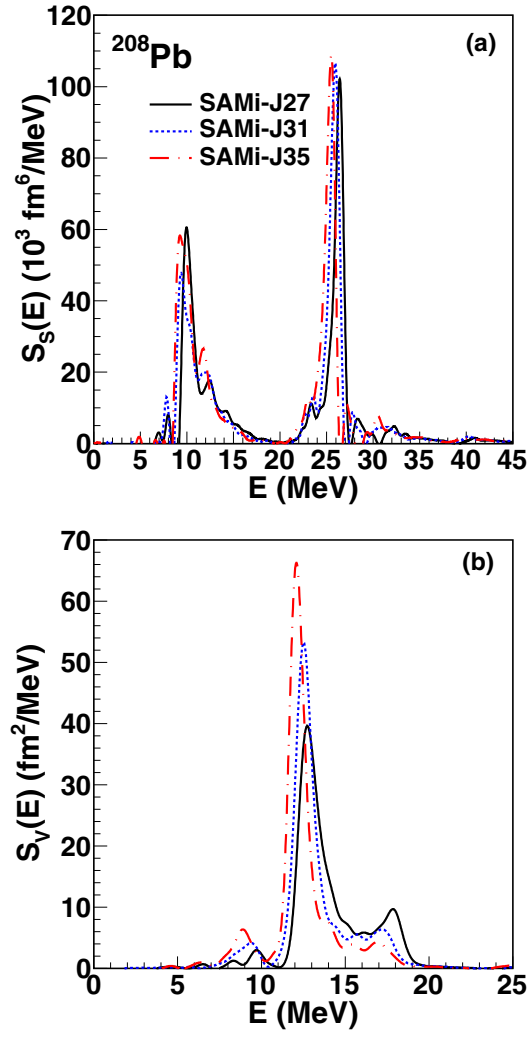

FIG. 6. Similar to Fig. 4 but for ^{208}Pb.

Let us concentrate now on the details of the isovector response. In the ^{208}Pb case, the centroid energies of the PDR as well as the energy peak of the isovector GDR predicted by the employed interactions ($E = 8$–10 MeV and $E = 12$–13 MeV, respectively) are close to the experimental data ($E = 7.37$ MeV within a window of 6–8 MeV [69] and $E = 13.43$ MeV with a total width of 2.42 MeV [70], respectively). The predictions of the three SAMi-J interactions for the PDR, for ^{132}Sn ($E = 9.0$–11.0 MeV) and for ^{68}Ni ($E = 11.5$–13.5 MeV), are also close, but still a little higher than the measured data ($E = 9.1$–10.5 MeV for ^{132}Sn [5,11] and $E = 11$ MeV with an energy width estimated to be less than 1 MeV for ^{68}Ni [10,71]). The overestimation of the PDR energy in our calculations may still be connected to the semiclassical treatment of surface effects, as already stressed above. Indeed the PDR region is essentially populated by low-lying isoscalar-like oscillations, whose energy is significantly affected by surface effects. The results can be probably improved by a fine tuning of the coefficients $C_{\rm surf}$ and $D_{\rm surf}$ in the Skyrme parametrizations.

Qualitatively, in the three nuclei it appears that the larger the value of L, the higher the different peaks arising in the low-energy region of the IV dipole response [see Figs. 4–6, panels (b)]. Moreover, as it clearly appears from panels (a), the strength of the lowest energy mode in the IS response increases (except for ^{208}Pb) when increasing the slope L of the parametrization considered. We note that, on the basis of nuclear matter calculations [40], we expect a larger degree of mixing between isoscalar and isovector modes, in neutron-rich systems, for symmetry energy parametrizations with larger slope L. Moreover, in this case, one also obtains a more extended neutron skin (see Fig. 2), thus surface and isospin effects are both enhanced.

Finally, we observe for all nuclei that the IV projection of the PDR is an order of magnitude smaller than the IV GDR, but its isoscalar counterpart is of the same order of magnitude as the corresponding IS GDR, in agreement with Ref. [34]. We conclude that the PDR region corresponds mostly to isoscalar low-energy modes, involving also nucleons which belong to the nuclear surface. Owing to the charge asymmetry of the systems considered, this mode also manifests an isovector

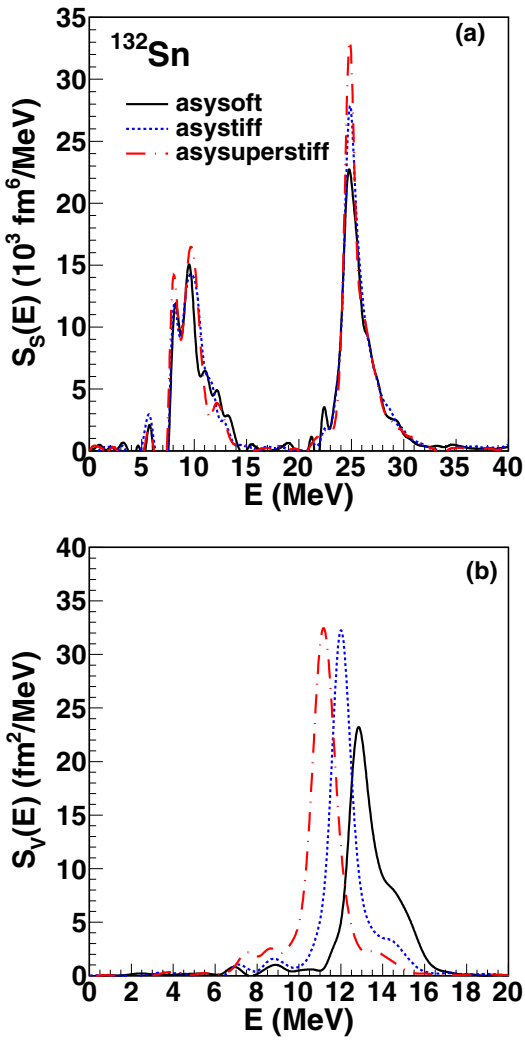

FIG. 7. Similar to Fig. 5, but for the MI interactions.

character, especially in the case of the stiffer interactions, which predict a larger asymmetry in the surface (neutron skin); see the density profile in Fig. 2.

Actually the IV response also exhibits other interesting features, which can be better discussed by comparing with the results obtained with the MI Skyrme interactions, displayed in Fig. 7 for ^{132}Sn. Concerning the main IV GDR, our calculations indicate that its excitation energy is mainly affected by the value of the symmetry energy at the density $\rho_c = 0.65\rho_0$, where the three SAMi-J interactions cross each other (see Fig. 1), which can be taken as the average density of medium-heavy nuclei. Indeed, the centroid of the IV GDR peak does not evolve much with the parametrization considered, in the SAMi-J case. The largest shift is observed for the smallest system, ^{68}Ni, indicating that the GDR centroid may be actually sensitive to the value of the symmetry energy at a density below ρ_c in this case. On the other hand, for the MI parametrizations, which cross at normal density (see Fig. 1), thus taking a smaller value of the symmetry energy below ρ_0 in the stiffer case, the energy centroid is clearly more sensitive to the parametrization employed (see Fig. 7) being smaller in the *asysuperstiff* case. We also stress that the GDR energy appears always underestimated by the MI interactions, whereas it is close to the experimental observation when the SAMi-J interactions are considered. In particular, the SAMi-J31 and the asystiff parametrizations are characterized by a quite similar behavior of the symmetry energy (compare the two panels of Fig. 1), nevertheless the results of the dipole response are different in the two cases. This highlights the role of momentum dependent effects in shaping the features of the nuclear response. One can also note that the energy location of the PDR strength is much less sensitive to the isovector channel of the interaction, especially in the MI case.

In the isovector dipole response obtained with the SAMi-J, we also observe a quite pronounced peak at higher energy, with respect to the GDR, whose strength decreases with the stiffness of the interaction, in agreement with RPA calculations [34]. This peak is less pronounced in the MI case.

As a test of the quality of our calculations, we have compared the numerically estimated value of the first moment $m_1 = \int_0^\infty E S_V(E) dE$ with the analytical energy weighted sum rule (EWSR). In the MI case, one can directly compare with the Thomas-Reiche-Kuhn (TRK) sum rule: $m_{1,TRK} = \hbar^2/(2m)NZ/A$. In the case of the SAMi-J interactions, one has to consider the enhancement factor for the sum rule, which is linked to the isovector effective mass [72,73], so that $m_1 = m_{1,TRK}(1 + k)$, where

$$k = \frac{2m}{\hbar^2}(C_{\text{eff}} - D_{\text{eff}})\frac{A}{NZ}\int d^3r \rho_n(r)\rho_p(r), \qquad (10)$$

$\rho_n(r)$ and $\rho_p(r)$ being the neutron and proton ground state densities, respectively. In all cases, the difference between numerical results and predicted values is within 5%. The EWSR exhausted by the PDR region can be calculated by integrating over the low-energy resonance area, taking as upper limit the energy corresponding to the minimum observed for the strength just below the GDR peak. The corresponding percentage of EWSR, f_y, is reported in Fig. 8 for the three systems and all the interactions (MI and MD) considered in our calculations. The values obtained with the MI interactions are quite close to the results reported in Ref. [53] and in the same range of the experimental observations [13]. One obtains systematically larger values for the MD interactions. This could be attributed to the contribution of mixed excitation modes [see for instance the peak around $E_2 = 11$ MeV in Fig. 5(a), for the ^{132}Sn case), whose energy, as discussed above, could be underestimated in our calculations [23,34]. In the calculations employing the MI interactions, this contribution is absorbed by the GDR strength, because also the GDR energies are underestimated [see Fig. 7(b)].

From the strength function, one can also calculate the nuclear dipole polarizability: $\alpha_D = 2e^2 \int_0^\infty S_V(E)/E dE$. In the case of ^{68}Ni, α_D varies from 4.7 to 5.4 fm^3 when we pass from the SAMi-J27 to the SAMi-J35 parametrization, whereas for ^{208}Pb it changes from 21.6 to 26.9 fm^3. Thus, for a given system, the larger the neutron skin thickness, the greater the value of the dipole polarizability. Experimentally, the dipole polarizability is below 4 fm^3 for ^{68}Ni [10] and around 20 fm^3 for ^{208}Pb [9]. The overestimation in our results reflects the

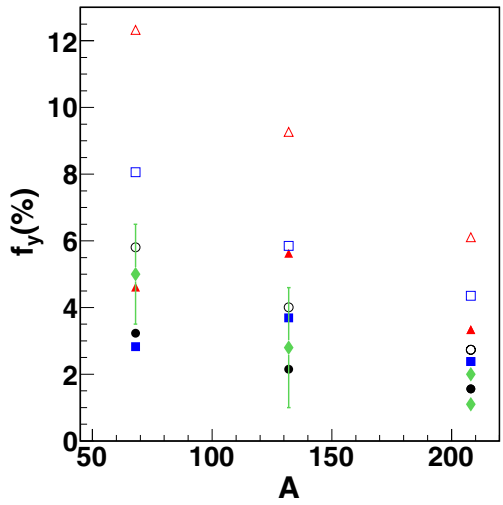

FIG. 8. The percentage of the EWSR exhausted by the PDR region (see text) for the three mass regions with MI and MD interactions and IV initial perturbation. The solid circles, squares, and triangles refer to the results for MI asysoft, asystiff, and asysuperstiff, interactions, respectively. The open circles, squares, and triangles refer to SAMi-J27, SAMi-J31, and SAMi-J35 and the diamonds refer to the experimental results [13], respectively.

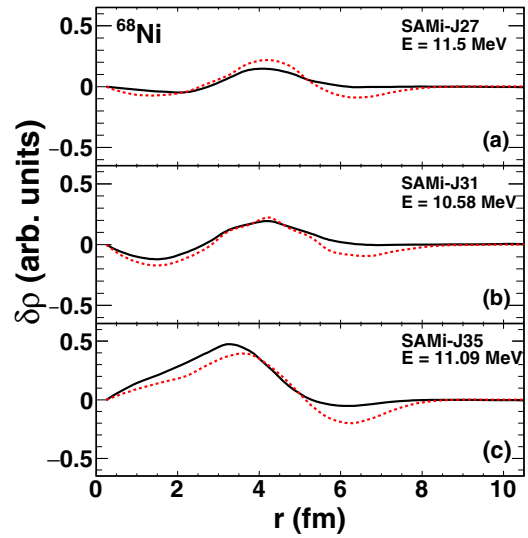

FIG. 9. The transition densities versus r in the low-energy excitation region, for the IS initial perturbation, for ^{68}Ni with SAMi-J27, SAMi-J31, and SAMi-J35 interactions. Full lines are for protons, dashed lines for neutrons. The energy of the excitation mode considered is indicated in each panel.

larger values obtained for the EWSR exhausted by the PDR with the SAMi-J interactions (see Fig. 8).

Finally, we mention that also for the IS strength our calculations fulfill, within 10%, the predicted EWSR [74].

B. Transition densities

In addition to the investigation of the dipole response presented above, the analysis of the transition densities associated with the different excitation modes of the system is very instructive since it delivers important information about the spatial structure related to the dynamics of every excitation.

To undertake this analysis, we need to evaluate the local spatial density as a function of time. In order to reduce numerical fluctuations, we take into account the cylindrical symmetry of the initial perturbation and, averaging over the azimuthal ϕ angle, we extract the density $\rho_q(r, \cos\theta, t)$ and the corresponding fluctuation $\delta\rho_q(r, \cos\theta, t) = \rho_q(r, \cos\theta, t) - \rho_q(r, t_0)$, where $\cos\theta = z/r$ and $\rho_q(r, t_0)$ denotes the ground state density profile which only depends on r.

As suggested in Ref. [52], assuming that the amplitude of the oscillation is weak (linear response regime), the spherical symmetry of the ground state and the dipole form of the excitation operator imply that the transition density can be written, at each time, as $\delta\rho_q(r, \cos\theta, t) = \delta\rho_q(r, t)\cos\theta$. Then one can finally extract the transition density just as a function of the radial distance r, by averaging, over $\cos\theta$, the quantity $\delta\rho_q(r, t) = \delta\rho_q(r, \cos\theta, t)/\cos\theta$.

It is clear that the delta function perturbation, $V_{\rm ext}$, at $t = t_0$, agitates simultaneously all modes which can be excited by the operator $\hat{D}_k$. Thus the corresponding density oscillations observed along the dynamical evolution will appear as the result of the combination of the different excitation modes. In order to pin down the contribution of a given mode to the density oscillations, one can consider the energy E associated, for instance, with a peak in the strength function and compute the transition density as the Fourier transform of $\delta\rho_q(r, t)$:

$$\delta\rho_q(r, E) \propto \int_{t_0}^{\infty} dt\, \delta\rho_q(r, t) \sin\frac{Et}{\hbar}. \tag{11}$$

In practice, since the simulation runs only to $t_{\rm max} = 1800\,{\rm fm}/c$, the sine function is multiplied by a damping factor, as in the strength function $S_k(E)$.

To further analyze the isoscalar or isovector character of each excitation mode, we calculate neutron and proton transition densities. It is well known that, in symmetric matter, neutrons and protons oscillate with exactly equal (isoscalar) or opposite (isovector) amplitudes. In neutron-rich systems, the picture is more complex; however, one can still identify isoscalar-like modes, when the two nuclear species oscillate in phase, and isovector-like modes, with neutrons and protons oscillating out of phase. Apart from this information, connected to the mixed character of each mode, the overall spatial structure of the transition densities tells us which part of the system (internal part, surface) is more involved in the oscillation.

In Figs. 9–11, we represent the transition density associated with the low-energy peaks observed in the isoscalar response, for the three systems considered and the three SAMi-J parametrizations adopted. As discussed above, owing to their mixed character, these modes also contribute to the isovector response, in the PDR region. The corresponding transition density could also be extracted from the isovector response; however, since the IV strength is quite small, numerical fluctuations would spoil the signal [75].

We observe that neutrons and protons oscillate in phase, but with different amplitudes, with neutrons having generally larger amplitude than protons. The nuclear surface is

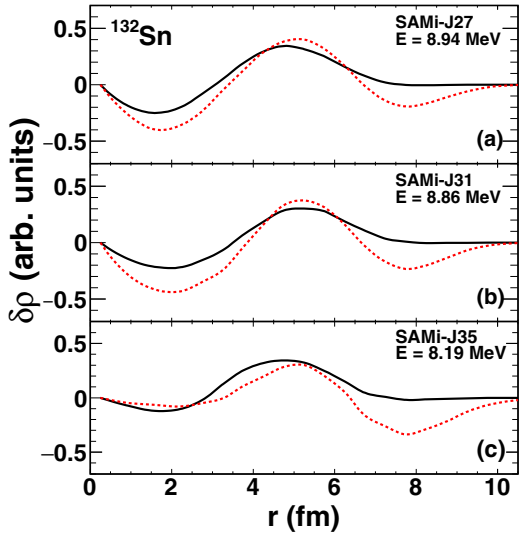

FIG. 10. Similar to Fig. 9 but for ^{132}Sn.

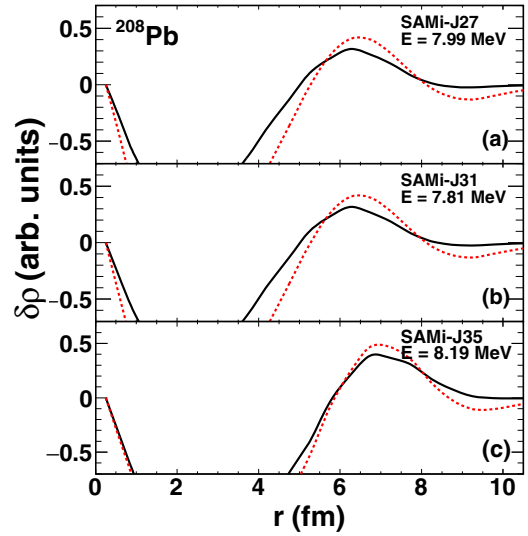

FIG. 12. Same as Fig. 11 but with a reduced scale on the vertical axis.

significantly involved in these oscillations. Moreover, when considering interactions with increasing slope L (from SAMi-J27 to SAMi-J35), one can see that neutron oscillations become larger, with respect to proton oscillations, especially in the surface region, whereas the opposite seems to hold for the interior of the system. This can be explained by the fact that, for increasing L, the system asymmetry is more pushed towards the surface, corresponding to the development of the neutron skin, whereas the internal part of the system becomes more symmetric. As one can see from Fig. 12, where the surface region of the transition density is better evidenced, surface effects are less pronounced in the ^{208}Pb case. However, a significant contribution to the dipole strength may also come from the intermediate spatial region, where the transition densities are positive. Indeed, according to the definition of the IV dipole moment, Eq. (7), the dipole strength increases when $\delta\rho_n/\delta\rho_p > N/Z$ for negative transition densities or when $\delta\rho_n/\delta\rho_p < N/Z$ for positive transition densities. Both conditions are better satisfied, in the surface and in the intermediate region respectively, with increasing L. This leads to an overall increase of the mixed character of the mode, mainly determined by the surface behavior, but also by the internal part of the system, explaining the larger strength observed in the isovector response; see Figs. 4–6.

We also extend our analysis to the other modes giving a relevant contribution to the isoscalar and the isovector responses. This is illustrated in Figs. 13 and 14 for the system ^{132}Sn, in the case of the SAMi-J31 interaction, for IS and IV excitations, respectively.

As it is observed from the analysis of the isoscalar response (Fig. 5), there exists a second mode, around $E_2 = 11$ MeV,

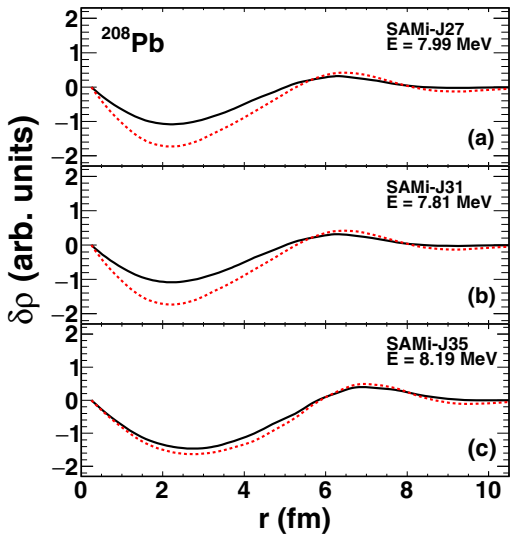

FIG. 11. Similar to Fig. 9 but for ^{208}Pb.

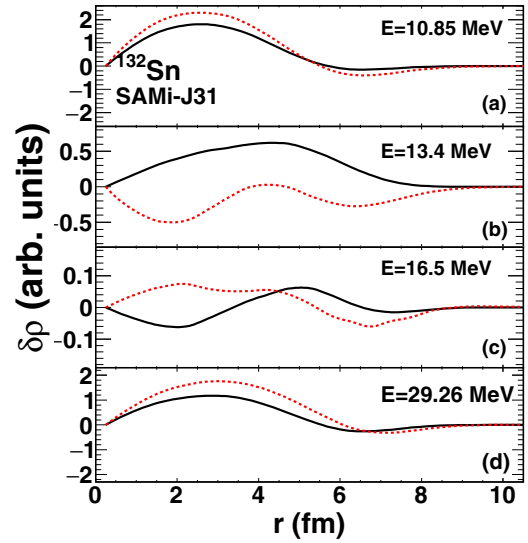

FIG. 13. The transition densities versus r with different excitation energies with IS initial perturbation for ^{132}Sn with SAMi-J31 interaction. Full lines are for protons, dashed lines for neutrons.

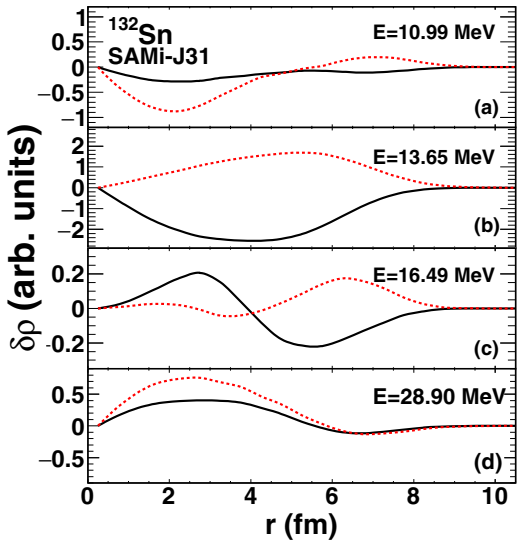

FIG. 14. Similar to Fig. 13 but with IV initial perturbation.

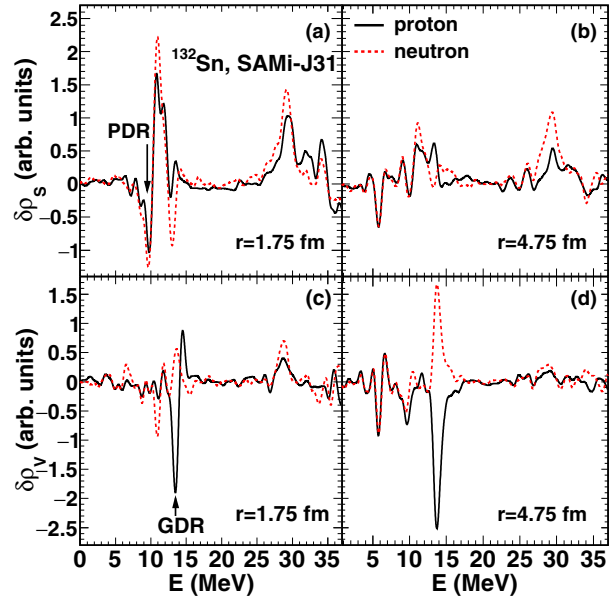

FIG. 15. Transition densities, as obtained considering an initial IS [(a) and (b)] or IV [(c) and (d)] perturbation, as a function of the excitation energy E, for ^{132}Sn and the SAMi-J31 interaction, at two radial distances: $r = 1.75$ fm and $r = 4.75$ fm.

which gives an important contribution in the low-energy region. This excitation also contributes to the isovector response, as already stressed in Sec. III A. Looking at the associated transition density, generated by an IS perturbation of the system [Fig. 13(a)], it appears that neutrons and protons essentially move in phase, but still with different amplitudes. Thus the oscillation has a mixed character and this is why it presents some strength in the isovector response. Now the interior of the system is more involved in the oscillation, though the surface is still affected. It is worth noting that, also for this transition density, the asymmetry increases with L at the surface and diminishes in the internal part.

We observe that, when this energy region is excited from the IV operator [Fig. 14(a)], although the structure of the mode remains similar, the difference between neutrons and protons becomes more pronounced. This effect could be due to the influence of the strong isovector oscillations associated with the IV GDR region, whose contribution may extend to the considered energy, so that GDR and PDR may overlap. Indeed, it should be noted that even if the energy E corresponds to a peak in $S_k(E)$, the transition densities obtained with the method employed here may still contain contributions from other modes if those have a width which makes their spectrum extend to the energy E [52]. It is interesting to note that the splitting of the PDR into a low-energy, mostly isoscalar contribution and a higher energy region with a more pronounced isovector character has been pointed out in recent experimental and theoretical analyses [16–18].

The highest energy isoscalar mode, that should be associated with the isoscalar giant dipole compression mode, corresponds to transition densities which affect significantly the interior of the system [Figs. 13 and 14, panels (d)] and its features do not depend much on the type of initial perturbation. Moreover it appears to be of quite robust isoscalar nature, with a small isoscalar-isovector mixing, especially at the surface.

It is also interesting to look at the modes which are isovector-like. In this case neutrons and protons oscillate mostly out of phase, with protons having larger amplitude. The transition densities extracted from the isoscalar or from the isovector responses exhibit similar features; compare panels (b) and (c) in Figs. 13 and 14. It appears that the main IV GDR mode [panels (b)] corresponds essentially to one oscillation, with a maximum close to the nuclear surface. This result is compatible with GT picture of neutron and proton spheres oscillating against each other. On the other hand, the higher energy peak, $E \approx 16.5$ MeV [panels (c)], corresponds to a kind of double oscillation, which is typical of SJ modes; i.e., volume oscillations, involving also the internal part of the system.

The full energy spectrum of transition densities, as obtained considering an initial IS [panels (a) and (b)] or IV [panels (c) and (d)] perturbation, at two radial distances is shown in Fig. 15 for the ^{132}Sn system and the SAMi-J31 interaction. One can observe that the low-energy region, on the left of the GDR peak, corresponds mostly to isoscalar-like excitations, where neutrons and protons move in phase. The same is seen at energies greater than $E \approx 17$ MeV. On the other hand, the energy region $E \approx 13$–17 MeV is clearly characterized by isovector-like excitation modes.

IV. CONCLUSIONS

In this work we have addressed some of the open questions concerning the nature of the low-lying IV dipole strength experimentally observed in neutron-rich nuclei [13], by performing a systematic investigation over three mass regions and employing effective interactions which mostly differ in the isovector channel. An essential point of our analysis is the examination of both IS and IV responses of the systems under study. Within our microscopic transport approach, a low-energy dipole collective mode occurs in the IV response of all investigated systems. The inspection of the IS response

in the same energy region reveals that the corresponding excitations are essentially isoscalar-like; i.e., neutrons and protons oscillate in phase but with different amplitude. This mechanism induces a finite, though small, isovector dipole moment oscillation, which is indeed revealed in the IV strength. These results are in agreement with the conclusions drawn from previous semiclassical investigations [52] or from RPA studies [30–34,76]. It is worth noticing that our analysis also indicates that, in neutron-rich systems, the modes which are mostly isovector (such as the IV GDR) also have a mixed character, thus contributing to the IS strength. This aspect, namely the mixing of isoscalar and isovector excitations in neutron-rich systems, has been widely discussed also in the context of infinite nuclear matter [40].

We also investigate how these features depend on the properties of the effective interaction considered and, in particular, on the density behavior of the symmetry energy. We observe that the strength associated with the collective pygmy dipole depends on the symmetry energy slope. The analysis of the corresponding transition densities reveals that this can be mostly related to the fact that the neutron-proton asymmetry of the nucleus increases with L at the surface, causing a larger mixing of isoscalar and isovector modes, which, in turn, increases the strength observed in the isovector response. One also observes that the asymmetry decreases with L in the internal part, also contributing to the dipole strength. Thus the neutrons which belong to the skin play an essential role in shaping the $E1$ response in the PDR region. However, this does not correspond to the oversimplified picture of the PDR, associated with the oscillations of the excess neutrons against an inert isospin symmetric core. Indeed, within our transport model, the dynamical simulations show a more complex structure of the modes contributing to the PDR [54], which also involves an excitation of the core in such a way that, inside the whole nucleus, neutrons and protons move in phase but with different amplitudes. It is also worth noticing that these low-lying isoscalar modes are observed also in symmetric systems, without a corresponding IV strength in this case [52].

By comparing with the results obtained with simpler MI interactions, we observe that the SAMi-J Skyrme parametrizations give a better reproduction of the centroid energy of the IV GDR, quite close to the experimental value. The results of our semiclassical approach are also quite close to RPA calculations [34]. On the other hand, the energy of the PDR looks overestimated, probably due to the semiclassical treatment of surface effects in our approach. Indeed low-energy excitations may be quite sensitive to surface properties, such as the structure of the nuclear density profile and the surface terms employed in the effective interaction. Clearly, semiclassical calculations are expected to yield some differences, with respect to quantum calculations, because of the lack of intrinsic gradient terms, apart from the effects originating from our numerical treatment. Moreover, because of the lack of shell effects, modes with low collectivity, associated with the excitation of single-particle states, which may also populate the PDR region [13], cannot be investigated within a semiclassical picture.

We consider that the results presented here, in particular the connection observed between the PDR strength, the mixed isoscalar-isovector character of the nuclear excitations, and the nuclear density profile, can be useful for further, systematic experiments searching for this quite elusive mode [16]. In particular, the features emerging from the analysis of the transition densities may help to select the best experimental conditions to probe the nuclear response in the PDR region. Moreover, a precise estimate of the strength acquired by the PDR in the dipole response can provide indications about the neutron skin extension, helping to constrain yet unknown properties of the nuclear effective interaction, namely the density dependence of the symmetry energy.

ACKNOWLEDGMENTS

We warmly thank X. Roca-Maza, E. G. Lanza, and G. Colò for enlightening discussions. The work by V. Baran was supported by a grant of the Romanian National Authority for Scientific Research, CNCS-UEFISCDI,Project No. PN-II-ID-PCE-2011-3-0972. This project has received funding from the European Unions Horizon 2020 Research and Innovation Programme under Grant Agreement No. 654002.

[1] M. N. Harakeh and A. van der Woude, *Giant Resonances*, Oxford Studies in Nuclear Physics Vol. 24 (Oxford University Press, New York, 2001).

[2] T. Hartmann, J. Enders, P. Mohr, K. Vogt, S. Volz, and A. Zilges, Phys. Rev. Lett. **85**, 274 (2000).

[3] T. Hartmann, J. Enders, P. Mohr, K. Vogt, S. Volz, and A. Zilges, Phys. Rev. C **65**, 034301 (2002).

[4] T. Kondo, H. Utsunomiya, S. Goriely, I. Daoutidis, C. Iwamoto, H. Akimune, A. Okamoto, T. Yamagata, M. Kamata, O. Itoh, H. Toyokawa, Y. W. Lui, H. Harada, F. Kitatani, S. Hilaire, and A. J. Koning, Phys. Rev. C **86**, 014316 (2012).

[5] P. Adrich, A. Klimkiewicz, M. Fallot, K. Boretzky, T. Aumann, D. Cortina-Gil, U. DattaPramanik, T. W. Elze, H. Emling, H. Geissel, M. Hellstrom, K. L. Jones, J. V. Kratz, R. Kulessa, Y. Leifels, C. Nociforo, R. Palit, H. Simon, G. Surowka, K. Summerer, and W. Walus, Phys. Rev. Lett. **95**, 132501 (2005).

[6] A. Klimkiewicz, N. Paar, P. Adrich, M. Fallot, K. Boretzky, T. Aumann, D. Cortina-Gil, U. Datta Pramanik, T. W. Elze, H. Emling, H. Geissel, M. Hellstrom, K. L. Jones, J. V. Kratz, R. Kulessa, C. Nociforo, R. Palit, H. Simon, G. Surowka, K. Summerer, D. Vretenar, and W. Walus, Phys. Rev. C **76**, 051603(R) (2007).

[7] A. Carbone, G. Colo, A. Bracco, L. G. Cao, P. F. Bortignon, F. Camera, and O. Wieland, Phys. Rev. C **81**, 041301(R) (2010).

[8] O. Wieland and A. Bracco, Prog. Part. Nucl. Phys. **66**, 374 (2011).

[9] A. Tamii, I. Poltoratska, P. von Neumann-Cosel, Y. Fujita, T. Adachi, C. A. Bertulani, J. Carter, M. Dozono, H. Fujita, K. Fujita, K. Hatanaka, D. Ishikawa, M. Itoh, T. Kawabata, Y. Kalmykov, A. M. Krumbholz, E. Litvinova, H. Matsubara, K. Nakanishi, R. Neveling, H. Okamura, H. J. Ong, B. Ozel-Tashenov, V. Y. Ponomarev, A. Richter, B. Rubio, H. Sakaguchi,

Y. Sakemi, Y. Sasamoto, Y. Shimbara, Y. Shimizu, F. D. Smit, T. Suzuki, Y. Tameshige, J. Wambach, R. Yamada, M. Yosoi, and J. Zenihiro, Phys. Rev. Lett. **107**, 062502 (2011).
[10] D. M. Rossi, P. Adrich, F. Aksouh, H. Alvarez-Pol, T. Aumann, J. Benlliure, M. Bohmer, K. Boretzky, E. Casarejos, M. Chartier, A. Chatillon, D. Cortina-Gil, U. Datta Pramanik, H. Emling, O. Ershova, B. Fernandez-Dominguez, H. Geissel, M. Gorska, M. Heil, H. T. Johansson, A. Junghans, A. Kelic-Heil, O. Kiselev, A. Klimkiewicz, J. V. Kratz, R. Krucken, N. Kurz, M. Labiche, T. LeBleis, R. Lemmon, Y. A. Litvinov, K. Mahata, P. Maierbeck, A. Movsesyan, T. Nilsson, C. Nociforo, R. Palit, S. Paschalis, R. Plag, R. Reifarth, D. Savran, H. Scheit, H. Simon, K. Summerer, A. Wagner, W. Walus, H. Weick, and M. Winkler, Phys. Rev. Lett. **111**, 242503 (2013).
[11] H. K. Toft, A. C. Larsen, A. Burger, M. Guttormsen, A. Gorgen, H. T. Nyhus, T. Renstrom, S. Siem, G. M. Tveten, and A. Voinov, Phys. Rev. C **83**, 044320 (2011).
[12] T. Aumann and T. Nakamura, Phys. Scr. T **152**, 014012 (2013).
[13] D. Savran, T. Aumann, and A. Zilges, Prog. Part. Nucl. Phys. **70**, 210 (2013).
[14] N. Paar, D. Vretenar, E. Khan, and G. Colò, Rep. Prog. Phys. **70**, 691 (2007).
[15] E. G. Lanza, A. Vitturi, M. V. Andrés, F. Catara, and D. Gambacurta, Phys. Rev. C **84**, 064602 (2011).
[16] F. C. L. Crespi *et al.*, Phys. Rev. Lett. **113**, 012501 (2014).
[17] E. G. Lanza, A. Vitturi, E. Litvinova, and D. Savran, Phys. Rev. C **89**, 041601 (2014).
[18] J. Endres, D. Savran, P. A. Butler, M. N. Harakeh, S. Harissopulos, R. D. Herzberg, R. Krucken, A. Lagoyannis, E. Litvinova, N. Pietralla, V. Y. Ponomarev, L. Popescu, P. Ring, M. Scheck, F. Schluter, K. Sonnabend, V. I. Stoica, H. J. Wortche, and A. Zilges, Phys. Rev. C **85**, 064331 (2012).
[19] A. Repko, P.-G. Reinhard, V. O. Nesterenko, and J. Kvasil, Phys. Rev. C **87**, 024305 (2013).
[20] P. Papakonstantinou, H. Hergert, and R. Roth, Phys. Rev. C **92**, 034311 (2015).
[21] F. Knapp, N. LoIudice, P. Vesely, F. Andreozzi, G. De Gregorio, and A. Porrino, Phys. Rev. C **92**, 054315 (2015).
[22] F. Knapp, N. LoIudice, P. Vesely, F. Andreozzi, G. De Gregorio, and A. Porrino, Phys. Rev. C **90**, 014310 (2014).
[23] N. Auerbach, C. Stoyanov, M. R. Anders, and S. Shlomo, Phys. Rev. C **89**, 014335 (2014).
[24] Y. Suzuki, K. Ikeda, and H. Sato, Prog. Theor. Phys. **83**, 180 (1990).
[25] P. Van Isacker, M. A. Nagarajan, and D. D. Warner, Phys. Rev. C **45**, R13 (1992).
[26] N. Tsoneva, H. Lenske, and Ch. Stoyanov, Phys. Lett. B **586**, 213 (2004).
[27] N. Tsoneva and H. Lenske, Phys. Rev. C **77**, 024321 (2008).
[28] N. Paar, P. Ring, T. Nikšić, and D. Vretenar, Phys. Rev. C **67**, 034312 (2003).
[29] D. Vretenar, N. Paar, P. Ring, and G. A. Lalazissis, Nucl. Phys. A **692**, 496 (2001); D. Vretenar, T. Nikšić, N. Paar, and P. Ring, *ibid.* **731**, 281 (2004).
[30] E. Litvinova, P. Ring, V. Tselyaev, and K. Langanke, Phys. Rev. C **79**, 054312 (2009).
[31] I. Daoutidis and P. Ring, Phys. Rev. C **83**, 044303 (2011).
[32] G. Cò, V. De Donno, C. Maieron, M. Anguiano, and A. M. Lallena, Phys. Rev. C **80**, 014308 (2009).
[33] E. Yükeel, E. Khan, and K. Bozkurt, Nucl. Phys. A **877**, 35 (2012).
[34] X. Roca-Maza, G. Pozzi, M. Brenna, K. Mizuyama, and G. Colò, Phys. Rev. C **85**, 024601 (2012).
[35] D. Sarchi, P. F. Bortignon, and G. Colò, Phys. Lett. B **601**, 27 (2004).
[36] S. Goriely, E. Khan, and M. Samyn, Nucl. Phys. A **739**, 331 (2004).
[37] N. Tsoneva, S. Goriely, H. Lenske, and R. Schwengner, Phys. Rev. C **91**, 044318 (2015).
[38] E. Litvinova, H. P. Loens, K. Langanke, G. Martinez-Pinedo, T. Rauscher, P. Ring, F.-K. Thielemann, and V. Tselyaev, Nucl. Phys. A **823**, 26 (2009).
[39] I. Daoutidis and S. Goriely, Phys. Rev. C **86**, 034328 (2012).
[40] V. Baran, M. Colonna, V. Greco, and M. Di Toro, Phys. Rep. **410**, 335 (2005).
[41] M. Colonna *et al.*, Eur. Phys. J. A **50**, 30 (2014).
[42] G. Giuliani, H. Zheng, and A. Bonasera, Prog. Part. Nucl. Phys. **76**, 116 (2014).
[43] A. W. Steiner, M. Prakash, J. M. Lattimer, and P. J. Ellis, Phys. Rep. **411**, 325 (2005).
[44] B.-A. Li, L.-W. Chen, and C. M. Ko, Phys. Rep. **464**, 113 (2008).
[45] S. Burrello, F. Gulminelli, F. Aymard, M. Colonna, and A. R. Raduta, Phys. Rev. C **92**, 055804 (2015).
[46] M. Goldhaber and E. Teller, Phys. Rev. **74**, 1046 (1948).
[47] H. Steinwedel, J. H. D. Jensen, and P. Jensen, Phys. Rev. **79**, 1019 (1950).
[48] D. M. Brink, A. Dellafiore, and M. Di Toro, Nucl. Phys. A **456**, 205 (1986).
[49] G. F. Burgio and M. Di Toro, Nucl. Phys. A **476**, 189 (1988).
[50] V. I. Abrosimov, A. Dellafiore, and F. Matera, Nucl. Phys. A **697**, 748 (2002).
[51] X. Roca-Maza, G. Colò, and H. Sagawa, Phys. Rev. C **86**, 031306(R) (2012); X. Roca-Maza *et al.*, *ibid.* **87**, 034301 (2013).
[52] M. Urban, Phys. Rev. C **85**, 034322 (2012).
[53] V. Baran, M. Colonna, M. Di Toro, A. Croitoru, and D. Dumitru, Phys. Rev. C **88**, 044610 (2013).
[54] V. Baran, B. Frecus, M. Colonna, and M. Di Toro, Phys. Rev. C **85**, 051601 (2012).
[55] Ad. R. Raduta *et al.*, Eur. Phys. J. A **50**, 24 (2014).
[56] L. G. Cao, G. Colò, and H. Sagawa, Phys. Rev. C **81**, 044302 (2010)
[57] R. B. Wiringa, V. Fiks, and A. Fabrocini, Phys. Rev. C **38**, 1010 (1988).
[58] C. Y. Wong, Phys. Rev. C **25**, 1460 (1982).
[59] D. Idier, B. Benhassine, M. Farine, B. Remaud, and F. Sebille, Nucl. Phys. A **564**, 204 (1993).
[60] P. Schuck *et al.*, Prog. Part. Nucl. Phys. **22**, 181 (1989).
[61] A. Guarnera, M. Colonna, and Ph. Chomaz, Phys. Lett. B **373**, 267 (1996).
[62] C. W. De Jager *et al.*, At. Data Nucl. Data Tables **36**, 495 (1987); G. Audi and A. H. Wapstra, Nucl. Phys. A **595**, 409 (1995); I. Angeli and K. P. Marinova, At. Data Nucl. Data Tables **99**, 69 (2013).
[63] X. Roca-Maza (private communication).
[64] F. Calvayrac, P. G. Reinhard, and E. Suraud, Ann. Phys. (N.Y.) **255**, 125 (1997).
[65] V. I. Abrosimov and O. I. Davydovs'ka, Ukr. J. Phys. **54**, 1068 (2009); V. Baran *et al.*, Rom. J. Phys. **57**, 36 (2012).
[66] P.-G. Reinhard, P. D. Stevenson, D. Almehed, J. A. Maruhn, and M. R. Strayer, Phys. Rev. E **73**, 036709 (2006).
[67] M. Uchida, H. Sakaguchi, M. Itoh, M. Yosoi, T. Kawabata, Y. Yasuda, H. Takeda, T. Murakami, S. Terashima, S. Kishi,

U. Garg, P. Boutachkov, M. Hedden, B. Kharraja, M. Koss, B. K. Nayak, S. Zhu, M. Fujiwara, H. Fujimura, H. P. Yoshida, K. Hara, H. Akimune, and M. N. Harakeh, Phys. Rev. C **69**, 051301(R) (2004); Y. W. Lui *et al.*, Nucl. Phys. A **731**, 28 (2004); G. Colò, N. Van Giai, P. F. Bortignon, and M. R. Quaglia, Phys. Lett. B **485**, 362 (2000).

[68] S. Ayik, M. Colonna, and P. Chomaz, Phys. Lett. B **353**, 417 (1995).

[69] N. Ryezayeva, T. Hartmann, Y. Kalmykov, H. Lenske, P. von Neumann-Cosel, V. Y. Ponomarev, A. Richter, A. Shevchenko, S. Volz, and J. Wambach, Phys. Rev. Lett. **89**, 272502 (2002).

[70] B. L. Berman and S. C. Fultz, Rev. Mod. Phys. **47**, 713 (1975).

[71] O. Wieland *et al.*, Phys. Rev. Lett. **102**, 092502 (2009).

[72] E. Lipparini and S. Stringari, Phys. Rep. **175**, 103 (1989).

[73] T. Oishi, M. Kortelainen, and N. Hinohara, Phys. Rev. C **93**, 034329 (2016).

[74] M. N. Harakeh and A. E. L. Dieperink, Phys. Rev. C **23**, 2329 (1981).

[75] R. Tabacu, M. C. Raportaru, E. Slusanschi, V. Baran, and A. I. Nicolin, Rom. J. Phys. **60**, 1441 (2015).

[76] V. Baran, D. I. Palade, M. Colonna, M. Di Toro, A. Croitoru, and A. I. Nicolin, Phys. Rev. C **91**, 054303 (2015).